7. S. D. Ling, C. R. Johnson, S. D. Frusher, K. R. Ridgway, *Proc. Natl. Acad. Sci. U.S.A.* **106**, 22341–22345 (2009).
8. T. Wernberg *et al.*, *Ecol. Lett.* **13**, 685–694 (2010).
9. N. A. J. Graham, S. Jennings, M. A. MacNeil, D. Mouillot, S. K. Wilson, *Nature* **518**, 94–97 (2015).
10. S. Bennett, T. Wernberg, E. S. Harvey, J. Santana-Garcon, B. J. Saunders, *Ecol. Lett.* **18**, 714–723 (2015).
11. E. S. Poloczanska *et al.*, *Nat. Clim. Change* **3**, 919–925 (2013).
12. T. Wernberg *et al.*, *Curr. Biol.* **21**, 1828–1832 (2011).
13. A. Vergés *et al.*, *Proc. Biol. Sci.* **281**, 20140846 (2014).
14. Materials and methods are available as supplementary materials on *Science* Online.
15. A. Hobday, G. Pecl, *Rev. Fish Biol. Fish.* **24**, 415–425 (2014).
16. M. T. Burrows *et al.*, *Science* **334**, 652–655 (2011).
17. T. Wernberg *et al.*, *Nat. Clim. Change* **3**, 78–82 (2013).
18. J. Zinke *et al.*, *Nat. Commun.* **5**, 3607 (2014).
19. J. Lough, A. Sen Gupta, A. J. Hobday, in *Report Card of Marine Climate Change for Australia: Detailed Scientific Assessment*, E. S. Poloczanska, A. J. Hobday, A. J. Richardson, Eds. (Hobart, Tasmania, 2012); www.oceanclimatechange.org.au.
20. S. Bennett, T. Wernberg, B. Arackal Joy, T. de Bettignies, A. H. Campbell, *Nat. Commun.* **6**, 10280 (2015).
21. D. P. Thomson, R. C. Babcock, M. A. Vanderklift, G. Symonds, J. R. Gunson, *Estuar. Coast. Shelf Sci.* **96**, 105–113 (2012).
22. M. Feng, D. Slawinski, L. E. Beckley, J. K. Keesing, *Mar. Freshw. Res.* **61**, 1259–1267 (2010).
23. M. A. Coleman *et al.*, *J. Ecol.* **99**, 1026–1032 (2011).
24. M. Feng, M. J. McPhaden, S.-P. Xie, J. Hafner, *Scientific Reports* **3**, 1277 (2013).
25. W. Cai *et al.*, *Nat. Clim. Change* **5**, 132–137 (2015).
26. B. D. Toohey, G. A. Kendrick, E. S. Harvey, *Oikos* **116**, 1618–1630 (2007).
27. P. K. Dayton, M. J. Tegner, *Science* **224**, 283–285 (1984).
28. E. A. Martinez, L. Cardenas, R. Pinto, *J. Phycol.* **39**, 504–508 (2003).
29. M. T. Burrows *et al.*, *Nature* **507**, 492–495 (2014).
30. S. Bennett *et al.*, *Mar. Freshw. Res.* **67**, 47–56 (2016).

STRUCTURAL BIOLOGY

Structural basis for membrane anchoring of HIV-1 envelope spike

Jyoti Dev,[1,2]* Donghyun Park,[3]* Qingshan Fu,[1] Jia Chen,[3,4] Heather Jiwon Ha,[3,4] Fadi Ghantous,[5] Tobias Herrmann,[2] Weiting Chang,[3] Zhijun Liu,[6] Gary Frey,[3,4] Michael S. Seaman,[5] Bing Chen,[3,4]† James J. Chou[1,6]

HIV-1 envelope spike (Env) is a type I membrane protein that mediates viral entry. We used nuclear magnetic resonance to determine an atomic structure of the transmembrane (TM) domain of HIV-1 Env reconstituted in bicelles that mimic a lipid bilayer. The TM forms a well-ordered trimer that protects a conserved membrane-embedded arginine. An amino-terminal coiled-coil and a carboxyl-terminal hydrophilic core stabilize the trimer. Individual mutations of conserved residues did not disrupt the TM trimer and minimally affected membrane fusion and infectivity. Major changes in the hydrophilic core, however, altered the antibody sensitivity of Env. These results show how a TM domain anchors, stabilizes, and modulates a viral envelope spike and suggest that its influence on Env conformation is an important consideration for HIV-1 immunogen design.

H IV-1 envelope spike [Env; trimeric (gp160)$_3$, cleaved to (gp120/gp41)$_3$] fuses viral and host cell membranes to initiate infection (*1*). Binding of gp120 to receptor (CD4) and co-receptor (e.g., CCR5 or CXCR4) trigger large conformational changes, leading to a cascade of refolding events in gp41 and ultimately to membrane fusion (*2–4*). Mature Env spikes, (gp120/gp41)$_3$, are the sole antigens on the virion surface; they often induce strong antibody responses in infected individuals (*5*, *6*). A vast amount of structural information is available for the ectodomain of Env, a primary target of the host immune system, but much less for its transmembrane domain (TMD), membrane-proximal external region (MPER), and cytoplasmic tail (CT), in the context of lipid bilayer. The cryo-EM (electron microscopy) structure of a detergent-solubilized clade B JR-FL EnvΔCT construct without the CT has been described recently (*7*), but its MPER and TMD are disordered, probably because detergent micelles failed to mimic a membrane environment.

The HIV-1 TMD is more conserved than a typical membrane anchor (fig. S1). Previous studies showed that mutations and truncations in the TMD indeed affect membrane fusion and viral infectivity (*8–11*). Presence of a GxxxG motif, often implicated in oligomeric assembly of TM helices (*12*), suggests clustering of TMDs in membrane (fig. S1). The presence of a conserved, positively charged residue (usually arginine) near the middle of the TMD suggests functions other than just spanning a bilayer. TM helices of many cell surface receptors are not merely inert anchors but play essential roles in receptor assembly and signal transmission. For example, we have shown that CT truncation affects the antigenic surface of the ectodomain of HIV-1 Env on the opposite side of the membrane (*13*). Thus, understanding the physical coupling (conformation and/or dynamics) between the CT and the ectodomain mediated by the TMD may guide design of immunogens that mimic native, functional Env and induce broadly neutralizing antibodies (bnAbs).

To characterize the TMD structure by nuclear magnetic resonance (NMR), we used a fragment of gp41 (residues 677 to 716; HXB2 numbering, fig. S1), derived from a clade D HIV-1 isolate 92UG024.2 (*14*). This construct, gp41$^{\text{HIV1D(677-716)}}$, contains a short stretch of MPER (residues 677 to 683); the TM segment (residues 684 to 705), defined by hydrophobicity; and a fragment previously assigned to the CT domain [residues 706 to 716, containing a tyrosine-based sorting motif (*15*, *16*)]. The gp41$^{\text{HIV1D(677-716)}}$ protein was purified and reconstituted into bicelles (fig. S2, A and B) (*17–19*) with an expected lipid-bilayer diameter of ~44 Å (fig. S2C) (*20*, *21*), thereby incorporating the refolded gp41$^{\text{HIV1D(677-716)}}$ into a membrane-like environment. The bicelle-reconstituted gp41$^{\text{HIV1D(677-716)}}$ migrated on SDS–polyacrylamide gel electrophoresis (SDS-PAGE) with a size close to that of a trimer (theoretical molecular mass 14.1 kDa) (fig. S2D), suggesting that the protein was trimeric and resistant to SDS denaturation. The reconstituted gp41$^{\text{HIV1D(677-716)}}$ protein in bicelles generated an NMR spectrum with excellent chemical-shift dispersion (fig. S3A). The equivalent protein constructs from isolates 92BR025.9 (clade C) and 92RU131.16 (clade G) gave similar NMR spectra (fig. S3, B and C), suggesting that the TMDs of most HIV-1 Envs have similar structures when reconstituted in bicelles. We completed the NMR structure of gp41$^{\text{HIV1D(677-716)}}$ using a previously described protocol (figs. S4 and S5) (*22*, *23*). The final ensemble of structures converged to a root mean

[1]Department of Biological Chemistry and Molecular Pharmacology, Harvard Medical School, 250 Longwood Avenue, Boston, MA 02115, USA. [2]Virology Program, Harvard Medical School, 260 Longwood Avenue, Boston, MA 02115, USA. [3]Division of Molecular Medicine, Boston Children's Hospital, 3 Blackfan Street, Boston, MA 02115, USA. [4]Department of Pediatrics, Harvard Medical School, 300 Longwood Avenue, Boston, MA 02115, USA. [5]Center for Virology and Vaccine Research, Beth Israel Deaconess Medical Center, 330 Brookline Avenue, Boston, MA 02215, USA. [6]State Key Laboratory of Molecular Biology, National Center for Protein Science Shanghai, Shanghai Institute of Biochemistry and Cell Biology, Chinese Academy of Sciences, Shanghai 200031, China.
*These authors contributed equally to this work. †Corresponding author. Email: bchen@crystal.harvard.edu
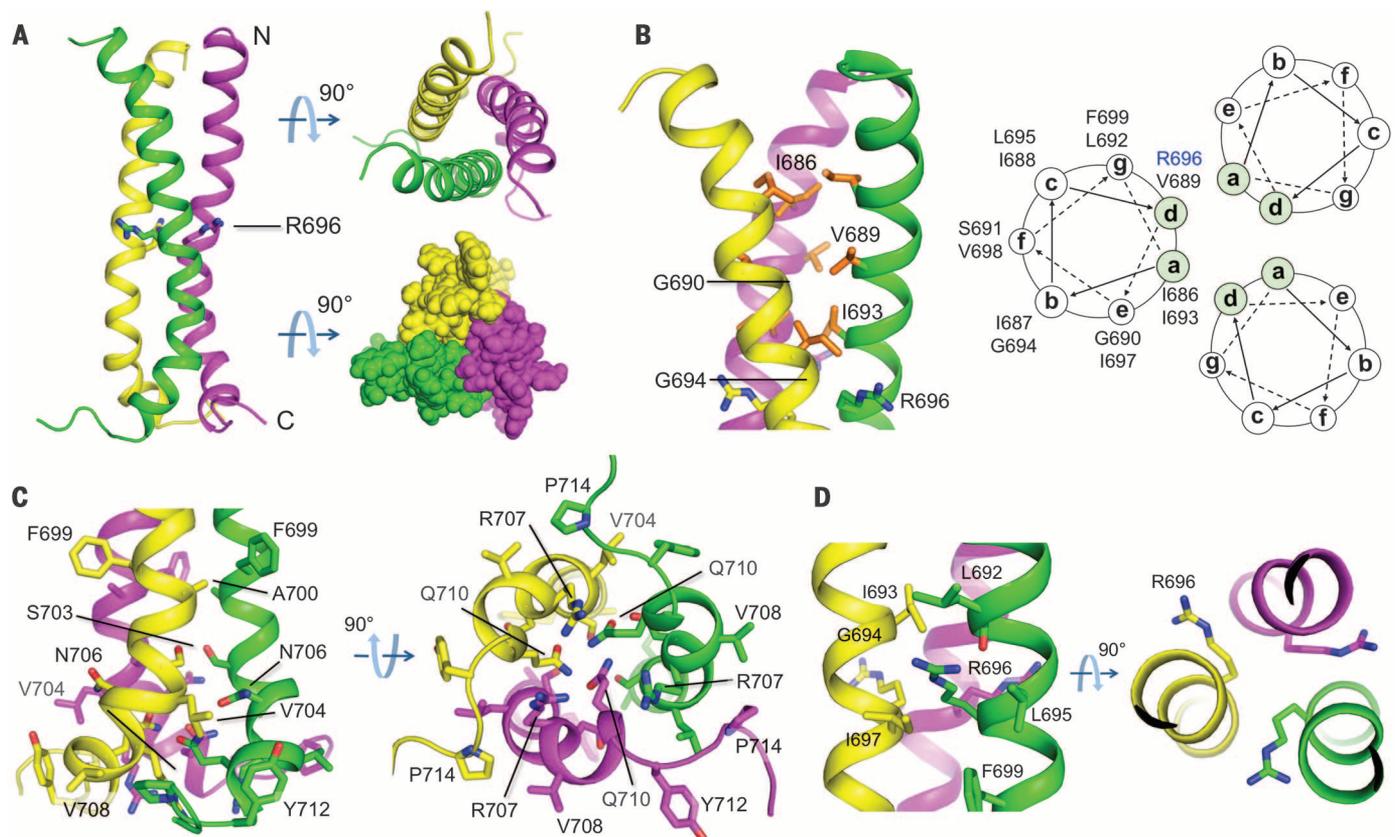
Fig. 1. NMR structure of the gp41^HIV1D(677-716) trimer in bicelles. (**A**) Ribbon representation of the lowest-energy structure from the calculated ensemble. The sphere representation of the top view (lower right) shows that the trimer has no ion-permeable holes. (**B**) The N-terminal half of the structure with hydrophobic residues (orange) arranged in the coiled-coil pattern (right panel). (**C**) The C-terminal half of the structure showing an array of polar residues that form the C-terminal hydrophilic core. The network of polar contacts is hypothesized to stabilize the trimer. (**D**) Enlarged middle region of the structure showing the intramembrane R696 and its surrounding hydrophobic residues, as well as the backbone oxygen of L692. Single-letter abbreviations for the amino acid residues are as follows: A, Ala; C, Cys; D, Asp; E, Glu; F, Phe; G, Gly; H, His; I, Ile; K, Lys; L, Leu; M, Met; N, Asn; P, Pro; Q, Gln; R, Arg; S, Ser; T, Thr; V, Val; W, Trp; and Y, Tyr.

square deviation of 0.95 and 1.44 Å for backbone and all heavy atoms, respectively (fig. S6 and table S1).

gp41^HIV1D(677-716) is a tightly assembled trimer ~54 Å long, with the conserved arginine (R696) near its midpoint (Fig. 1A). It shows a packing arrangement not seen in any other known TM helix dimers or trimers: Its N- and C-terminal halves have different modes of assembly, with an intervening kink. The N-terminal region is a conventional three-chain coiled-coil formed by residues 686 to 696 (Fig. 1B), including the GxxxG motif. The C-terminal half does not show classic "knobs-into-holes" interactions, but instead is held together by a network of polar contacts, mainly involving R707 and Q710, at the trimer interface of the kinked helical segments (residues 704 to 712) (Fig. 1C). We call this interface the "hydrophilic core."

R696, near the middle of each TM helix (Fig. 1D), produces three unbalanced charges at the center of the membrane. This residue occupies a "d" position in the heptad sequence (Fig. 1B). Its C$^\beta$ points toward the threefold axis of the trimer, while the rest of the side chain bends away from the axis, placing the guanidinium group in a peripheral hydrophobic pocket formed

by L692, L695, and I697 (Fig. 1D). The backbone carbonyl of L692 may form a hydrogen bond with one of the guanidinium NH$_2$ group of R696. H$^\varepsilon$ of R696 showed a water nuclear Overhauser effect (NOE) in a ^{15}N-edited NOE spectrum (fig. S4), indicating the presence of an adjacent structured water. Thus, the guanidinium group, presumably charged at pH 6.7 under the NMR conditions, is partially neutralized by hydrogen bonding with the electronegative backbone oxygen of L692 and the water molecule. The polarizability of the hydrophobic pocket that surrounds the guanidinium may also lower its pK_a (acid dissociation constant) from its value in aqueous solution. Although well accommodated in the TMD trimer, the intramembrane R696 may modulate the stability of the helical trimer if the helices dissociate at any stage in assembly or fusion. The ^{1}H-^{15}N correlation spectrum of the gp41^HIV1D(677-716) trimer showed inhomogeneous peak linewidth, with the N-terminal half near R696 having the most severe peak broadening, consistent with conformational fluctuation (fig. S7).

To confirm membrane partition of the TMD trimer, we used a paramagnetic probe, Gd(DOTA) (24), to measure solvent exposure of the four arginine residues in the gp41^HIV1D(677-716) trimer.

These arginines are distributed at different positions along the TM helices and thus serve as four depth markers. We measured intensity decrease of the arginine Hε-Nε correlation peaks at increasing concentrations of Gd(DOTA). The most solvent-exposed R707 showed the highest sensitivity to Gd(DOTA), whereas the most buried R696 was the least sensitive (Fig. 2A). R683 and R709 are near opposite lipid headgroup regions in the structure. R709 showed a greater resonance broadening than did R683, indicating that the latter is more deeply buried. We placed the gp41^HIV1D(677-716) trimer in the lipid bilayer so that the four arginine positions were consistent with their respective sensitivity to Gd(DOTA) (Fig. 2B). This placement, which is consistent with the surface distribution of hydrophobic, polar, and charged residues (Fig. 2C), places R696 in a fully hydrophobic environment, slightly closer to the cytoplasmic side of the membrane. The MPER segment is in the headgroup region of the outer leaflet. The C-terminal segment, previously assigned to the CT, is at the headgroup-water interface of the inner leaflet.

To assess the contribution of specific residues to TMD stability, we generated 12 gp41^HIV1D(677-716) mutants with single or double mutations, mainly
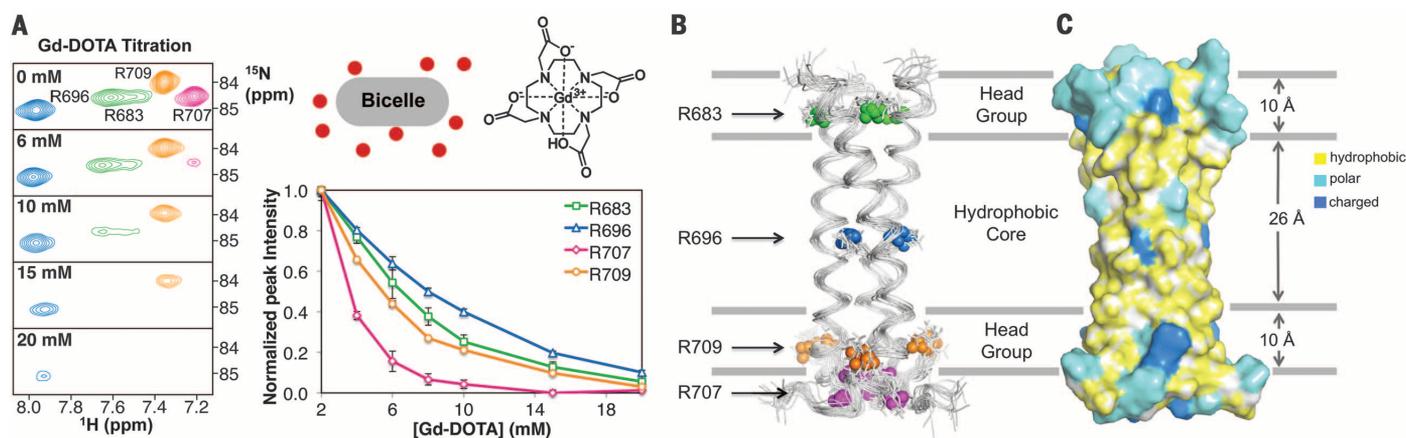
Fig. 2. Partition of the gp41^HIV1D(677-716) trimer in lipid bilayer. (**A**) Measurement of membrane immersion depth of the four arginines using the water-soluble and membrane-inaccessible paramagnetic probe Gd-DOTA. The ^1H-^{15}N correlation peaks of the arginine Hε-Nε recorded in q = 0.5 bicelles (left) showed reduced peak intensity with increasing Gd-DOTA concentration (right) due to paramagnetic relaxation enhancement (PRE). R683 is shown in green, R696 in blue, R707 in magenta, and R709 in orange. Error bars represent spectra noise level normalized against maximum reference peak intensity. (**B**) Placement of the trimer structure in the presumed DMPC lipid bilayer, which is slightly thinner than the characterized thickness of DOPC bilayer (35), such that the positions of the four arginines are in accordance with the PRE results in (A). The positions of the arginine side chains are indicated by the Hε (spheres) in the ensemble of 15 low-energy structures. The color scheme is the same as in (A). (**C**) Surface representation of the lowest-energy structure positioned in DMPC bilayer as in (B) for showing the surface distribution of hydrophobic, polar, and charged amino acids. The hydrophobic residues (yellow) include A, I, L, F, V, P, and G; the polar residues (cyan) include Q, N, H, S, T, Y, C, M, and W; the charged residues (blue) include K, R, D, and E.

in the trimer interface. To introduce large-scale changes in the hydrophilic core, we also created mutants Δ(705–716) and G690L/Δ(705–716) with residues 705 to 716 deleted, and mutants 704–713 and G690L/704–713 with residues 704 to 713 mutated (Fig. 3 and table S2). We analyzed these mutants by SDS-PAGE after reconstitution in bicelles (fig. S8). Most simple mutations, including I686A, I693A, and R696N, did not disrupt the trimer completely, but only shifted the band to molecular mass positions lower than that of the wild type, indicating only partial trimer de-stabilization (fig. S8). We observed a similar pattern for mutants 704–713, G690L/704–713, and Δ705–716. The only mutant that migrated as a monomer was G690L/Δ705–716, with the GxxxG motif mutated and the entire hydrophilic-core region truncated (fig. S8). Thus, both the coiled-coil and the hydrophilic core contribute to the extraordinary stability of the TMD, and either one of them is sufficient to prevent the trimer from complete dissociation in bicelles.

To elucidate functional roles of the structural elements in the TMD, we mutated each of them in the intact Env spike and analyzed the effect on Env biogenesis, membrane fusion, and viral infectivity. We generated 27 Env mutants, using the sequence of a clade A isolate 92UG037.8, with single, double, or triple mutations in the coiled-coil region, R696 and its protecting residues, the kink, the hydrophilic core, or combinations of these elements (table S2). We also produced mutants 704–713 and G690L/704–713. When transiently transfected in 293T cells, all mutants expressed comparable levels of Env, with similar extents of cleavage between gp120 and gp41, as well as similar cell-surface levels (figs. S9 and S10). At a high Env expression level, at which cell-cell fusion was resistant to most neutralizing antibodies,

the fusion activity of the TMD mutants was indistinguishable (93 to 109%) from that of the wild type (fig. S11). When the expression level was reduced to mimic the low surface density on HIV-1 virions (25), several TMD mutants, including R696A, had significantly lower cell-cell fusion activity than did the wild type (table S2 and fig. S12). Likewise, when these mutations were introduced into pseudoviruses, there were no major differences in Env incorporation and processing, but limited changes in infectivity for most of them (table S2 and figs. S13 and S14). R696A had almost full wild-type infectivity, whereas 704–713 and G690L/704–713 had substantially less—just the opposite of their effects on cell-cell fusion (table S2 and fig. S14).

To determine whether mutations in the TMD can influence the antigenic structure of the Env ectodomain and whether they might affect its antibody sensitivity, we used the cell-cell fusion assay to test inhibition of each Env mutant by a trimer-specific bnAb PG16 and by a nonneutralizing V3 antibody 3791 (table S3). Most mutants were essentially identical to the wild type in their sensitivity to either antibody; mutants I686A, Y712A, P714N, G690L/Y712A, G690L/P714N, G690L/P714K, and G690L/P714H exhibited detectable differences (fig. S15). We observed the most pronounced differences for mutants 704–713 and G690L/704–713, for which PG16 and 3791 switched phenotypes—the former became inactive and the latter inhibitory (fig. S15). All mutations that affect antibody inhibition are located in either the coiled-coil or the hydrophilic core. We infer that changes in TMD stability influence the antigenic structure of the ectodomain of the functional Env. When tested in a pseudovirus-based neutralization assay with bnAbs PG9 (trimer specific), 3BNC117 (CD4 binding site), 10-1074 (glycan- and V3-dependent),

10E8 (MPER), and 3791 (table S3), most mutants, except for 704–713 and G690/704–713, were unchanged in their sensitivity to PG9, 3BNC117, 10-1074 and 3791, but most became more sensitive to 10E8 (table S4). This result suggests that the changes produced by all the mutations tested, except for 704–713 and G690/704–713, are limited to local structure. In contrast, the mutants 704–713 and G690/704–713 became resistant to PG9 and sensitive to 3791—reflecting their properties in the cell-cell fusion assay. Mutant 704–713 was analyzed with additional antibodies. For cell-cell fusion, wild-type Env is sensitive to trimer-specific bnAbs PG9, PG16, and PGT145 and resistant to nonneutralizing antibodies b6 (CD4 binding site), 3791, and 17b (CD4-induced) (table S3, Fig. 3A, and fig. S16). The antibody inhibition pattern is reversed, however, for the fully functional mutant 704–713, indicating that the hydrophilic core of the TMD plays an important role in stabilizing and modulating the antigenic structure of the Env spike. Similar phenotypes were also observed with a 704–713 mutant derived from a clade C strain C97ZA012 (fig. S17). The pseudovirus neutralization assay gave similar, but less pronounced, results for the mutant 704–713 (Fig. 3B and table S4).

The most important finding from this study relevant to vaccine development is how the TMD modulates the antigenic surfaces of the Env spike. We reported previously that truncation of the CT domain of HIV-1 Env reshapes the antigenic surfaces of its ectodomain (13). We now show that mutations destabilizing the hydrophilic core of the TMD trimer resemble the CT deletion in altering the sensitivity of the functional Env to both nonneutralizing and trimer-specific neutralizing antibodies. In particular, the trimer-specific bnAbs, which neutralize by stabilizing the native

Fig. 3. Effect of mutations in the TMD of HIV-1 Env on its antibody sensitivity. (**A**) Antibody inhibition of cell-cell fusion mediated by the wild-type 92UG037.8 Env (left) and the TMD mutant 704–713 [right; residues 704 to 713 (VINRVRQGYS) were mutated to SSAASAAGSA] was analyzed with both nonneutralizing antibodies—including b6 (CD4 binding site; blue), 3791 (V3; cyan), and 17b (CD4-induced; purple)—and trimer-specific bnAbs, including PG9 (orange), PG16 (red), and PGT145 (magenta). The CD4 binding site bnAb VRC01 (green) was a control antibody. The experiment was carried out in triplicate and repeated at least twice with similar results. Error bars indicate the SD calculated by the Excel STDEV function. (**B**) Antibody neutralization of pseudoviruses containing either the 92UG037.8 Env (left) or the TMD mutant 704–713 (right) was determined with antibodies b6, 3791, 17b, PG9, PG16, and PGT145, shown in the same color scheme as in (A). The CD4 binding site bnAb 3BNC117 was a control antibody (green). The experiment was performed in duplicate.
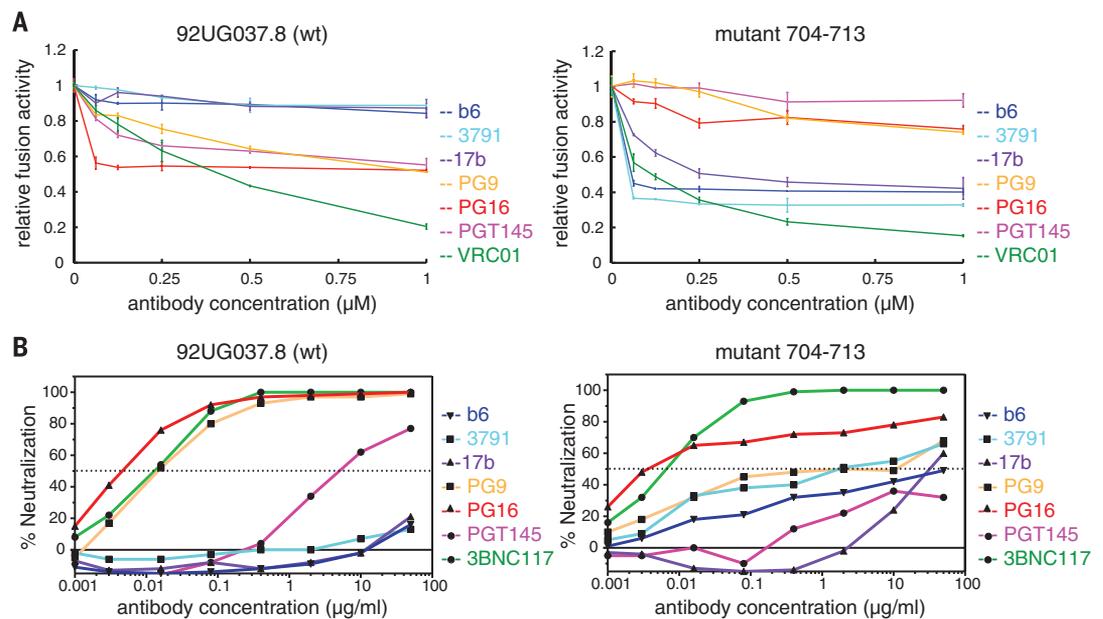
conformation of Env (*26, 27*), do not recognize the Env spike when its TMD has been destabilized. We suggest that the TMD mediates conformational coupling between the ectodomain and the CT and that the trimeric structure seen by NMR represents the conformation of the TMD adopted by a native Env spike in a membrane.

The placement of gp41$^{HIV1D(677-716)}$ in a lipid bilayer reveals clear boundaries of the TM segment and settles a contentious issue (*10, 28*). Part of the 10E8 epitope (residues 677 to 683) is embedded in the headgroup layer of the outer leaflet, consistent with lack of accessibility of this epitope on the native Env (*13, 29*). The hydrophilic core, which was thought to be part of the CT, is similarly protected by the headgroup layer of the inner leaflet. This hydrophilic region contains a tyrosine-based sorting signal (^{712}YSPL^{715}), which may participate in Env internalization by endocytosis (*15, 16, 30*). Our structure indicates that Y712 and P714 in this motif on one TM protomer interact with L704 and V708 of the adjacent protomer, respectively, thereby also contributing to trimer stability.

The TMD is required not only for membrane anchoring and fusion, but also for stability of the entire Env spike. This observation can explain why most soluble Env preparations with the TMD deleted, except for those of a few selected strains (*31, 32*), are unstable and conformationally heterogeneous, unless they have specific, stabilizing modifications (*26, 33, 34*). To design immunogens that mimic optimally native viral spikes, one must not ignore structural constraints imposed by the TMD on the ectodomain. The high-resolution structure of the HIV-1 Env TMD trimer presented here can be a guide for engineering more effective immunogens.

REFERENCES AND NOTES

1. S. C. Harrison, *Nat. Struct. Mol. Biol.* **15**, 690–698 (2008).
2. D. C. Chan, D. Fass, J. M. Berger, P. S. Kim, *Cell* **89**, 263–273 (1997).
3. W. Weissenhorn, A. Dessen, S. C. Harrison, J. J. Skehel, D. C. Wiley, *Nature* **387**, 426–430 (1997).
4. M. Pancera *et al.*, *Nature* **514**, 455–461 (2014).
5. X. Wei *et al.*, *Nature* **422**, 307–312 (2003).
6. D. D. Richman, T. Wrin, S. J. Little, C. J. Petropoulos, *Proc. Natl. Acad. Sci. U.S.A.* **100**, 4144–4149 (2003).
7. J. H. Lee, G. Ozorowski, A. B. Ward, *Science* **351**, 1043–1048 (2016).
8. R. J. Owens, C. Burke, J. K. Rose, *J. Virol.* **68**, 570–574 (1994).
9. L. Shang, L. Yue, E. Hunter, *J. Virol.* **82**, 5417–5428 (2008).
10. L. Yue, L. Shang, E. Hunter, *J. Virol.* **83**, 11588–11598 (2009).
11. E. Helseth *et al.*, *J. Virol.* **64**, 6314–6318 (1990).
12. M. G. Teese, D. Langosch, *Biochemistry* **54**, 5125–5135 (2015).
13. J. Chen *et al.*, *Science* **349**, 191–195 (2015).
14. F. Gao *et al.*, *J. Virol.* **70**, 1651–1667 (1996).
15. J. F. Rowell, P. E. Stanhope, R. F. Siliciano, *J. Immunol.* **155**, 473–488 (1995).
16. M. Boge, S. Wyss, J. S. Bonifacino, M. Thali, *J. Biol. Chem.* **273**, 15773–15778 (1998).
17. M. E. Call *et al.*, *Cell* **127**, 355–368 (2006).
18. M. E. Call, K. W. Wucherpfennig, J. J. Chou, *Nat. Immunol.* **11**, 1023–1029 (2010).
19. To produce the protein, we expressed the His-tagged TrpLE-gp41$^{HIV1D(677-716)}$ fusion protein in *Escherichia coli* as inclusion bodies, purified the solubilized protein by Ni-affinity chromatography, removed the TrpLE tag with cyanogen bromide, and separated the product by reverse-phase high-performance liquid chromatography. Bicelles were made of 1,2-dimyristoyl-sn-glycero-3-phosphocholine (DMPC; lipid) and 1,2-dihexanoyl-sn-glycero-3-phosphocholine (DHPC; detergent) at a ratio (*q*) of 0.5. In this report, we use gp41$^{HIV1D(677-716)}$ and TMD interchangeably for convenience.
20. K. J. Glover *et al.*, *Biophys. J.* **81**, 2163–2171 (2001).
21. C. R. Sanders 2nd, J. P. Schwonek, *Biochemistry* **31**, 8898–8905 (1992).
22. B. OuYang *et al.*, *Nature* **498**, 521–525 (2013).
23. For structure determination, we proceeded with the clade D construct because its expression level was the highest. The approach involves determination of local structures of the monomers and assembly of the trimer with intermonomer distance restraints derived from NOEs between structurally equivalent but isotopically differently labeled subunits. We could identify eight intermonomer NOEs using the isotopically mixed labeled sample to calculate a unique assembly solution, which was further validated and refined with other conventional NOE data.
24. Gd(DOTA) is a water-soluble and membrane-inaccessible molecule, so that the paramagnetic relaxation enhancement (PRE) it generates decreases with distance from the bilayer surface.
25. P. Zhu *et al.*, *Nature* **441**, 847–852 (2006).
26. R. W. Sanders *et al.*, *PLOS Pathog.* **9**, e1003618 (2013).
27. J. P. Julien *et al.*, *Proc. Natl. Acad. Sci. U.S.A.* **110**, 4351–4356 (2013).
28. J. T. West, P. B. Johnston, S. R. Dubay, E. Hunter, *J. Virol.* **75**, 9601–9612 (2001).
29. J. Chen *et al.*, *J. Virol.* **88**, 1249–1258 (2014).
30. C. Berlioz-Torrent *et al.*, *J. Virol.* **73**, 1350–1361 (1999).
31. S. A. Jeffs *et al.*, *Vaccine* **22**, 1032–1046 (2004).
32. J. M. Kovacs *et al.*, *Proc. Natl. Acad. Sci. U.S.A.* **111**, 18542–18547 (2014).
33. J. Guenaga *et al.*, *J. Virol.* **90**, 2806–2817 (2015).
34. Y. Do Kwon *et al.*, *Nat. Struct. Mol. Biol.* **22**, 522–531 (2015).
35. M. C. Wiener, S. H. White, *Biophys. J.* **61**, 434–447 (1992).

Editor's Summary

Env's transmembrane domain revealed

HIV-1's envelope protein (Env) spans the viral membrane and grants the virus entry into host cells. Env is also the sole protein of HIV-1 that is targeted by antibodies, making it a key target for vaccine design. Dev *et al.* used nuclear magnetic resonance to determine an atomic-level structure of the membrane-spanning region of Env in a lipid bicelle. Env's transmembrane domain forms a well-ordered trimer, which includes a stabilizing C-terminal hydrophilic core. Disrupting this core alters the sensitivity of Env to broadly neutralizing antibodies, suggesting the potential importance of this region to vaccine design.

Science, this issue p. 172

Article Tools	Visit the online version of this article to access the personalization and article tools: http://science.sciencemag.org/content/353/6295/172
Permissions	Obtain information about reproducing this article: http://www.sciencemag.org/about/permissions.dtl